Soil Dynamics and Earthquake Engineering 191 (2025) 109283

Contents lists available at ScienceDirect

Soil Dynamics and Earthquake Engineering

journal homepage: www.elsevier.com/locate/soildyn

# Sobol' sensitivity analysis of a 1D stochastic elasto-plastic seismic wave propagation

Hexiang Wang [a], Fangbo Wang [b], Han Yang [b], Katarzyna Staszewska [c], Boris Jeremić [d,*]

[a] Berkshire Hathaway Specialty Insurance, San Ramon, CA, USA
[b] Tianjin University, Tianjin, PR China
[c] Faculty of Civil and Environmental Engineering, Gdańsk University of Technology, Gdańsk, Poland
[d] University of California, Davis, CA, USA

ARTICLE INFO

*Keywords:*
Sensitivity analysis
Elasto-plastic seismic wave propagation
Stochastic ground motions
Uncertain soil properties
Sobol' indices
Stochastic FEM

ABSTRACT

A novel numerical framework for the Sobol' sensitivity analysis of 1D stochastic elasto-plastic wave propagation is proposed and evaluated. The forward propagation of uncertain input motions through uncertain elasto-plastic soils and structures is often conducted using the finite element method (FEM) together with the Monte Carlo simulation. However, it is computationally much more efficient to use the stochastic elasto-plastic FEM (SEPFEM) instead. Hence the developed framework is based on the SEPFEM. The backward propagation of uncertainties, that is, the determination of relative influences of individual uncertain input motions and uncertain material properties on the resulting uncertain seismic wave propagation, is known as the global sensitivity analysis. A global sensitivity analysis, namely, the Sobol' sensitivity analysis, is included in the proposed framework. Uncertain input, bedrock motions are obtained using the ground motion prediction equations of Fourier amplitude spectra and Fourier phase derivative, and they are modeled as a non-stationary random process. Stochastic elasto-plastic soil properties are represented as heterogeneous random fields. The random process and the random fields are discretized in the probabilistic space using an orthogonal Hermite polynomial chaos (PC) basis. The probabilistic system response is obtained efficiently using the Galerkin stochastic FEM. The Sobol' sensitivity analysis is conducted for the PC-represented uncertain system response. The benefits of the presented framework to the site-specific probabilistic seismic hazard analysis are discussed.

The novel approach enables to take into account the uncertainty in both, seismic load and elasto-plastic material parameters, and to assess their individual influences on the overall uncertainty in the resulting wave field accurately and efficiently. The presented framework has been implemented into Real-ESSI Simulator and, here, it is evaluated and demonstrated to be very useful for the seismic site response analysis.

## 1. Introduction

A seismic site response analysis deals with the ground surface motions that result from the input, bedrock seismic motions. The site response analysis is important in the estimation of seismic demands for planned engineering structures because it accounts for the local site effects. In the conventional seismic site response analyses, material parameters and input, bedrock motions [1] are assumed to be deterministic. However, soil parameters are inherently variable and uncertain [2–4]. Besides, significant variabilities of input, bedrock motions arise from uncertain seismic sources, uncertain wave propagation paths, etc. [5]. It is important to account for these uncertainties in seismic site response analyses [6,7].

In the recent years, the probabilistic modeling of seismic wave propagation, i.e., the forward propagation of uncertain input, bedrock motions through uncertain soils and through uncertain structures has been conducted using the finite element method (FEM), either together with the Monte Carlo simulation (MCS) [8,9] or, much more efficiently, together with the polynomial chaos (PC) expansion [10–12]. For example, Johari and Momeni [13] performed a stochastic analysis of ground response using non-recursive algorithm. In addition to the forward uncertainty propagation, the backward uncertainty propagation can be carried out, as well. In other words, it may be useful to determine the relative influences of uncertain input motions and uncertain material properties on the resulting probabilistic system response. This is possible using a global sensitivity analysis. A global sensitivity analysis enables the decomposition of the variance of the probabilistic output of the model into portions pertaining to the individual random inputs. In this study, a global sensitivity analysis of a stochastic seismic wave

* Corresponding author.
*E-mail address:* jeremic@ucdavis.edu (B. Jeremić).

https://doi.org/10.1016/j.soildyn.2025.109283
Received 17 May 2024; Received in revised form 13 January 2025; Accepted 28 January 2025
Available online 7 February 2025

propagation is conducted and it is used for the site response analysis.

Several global sensitivity measures have been proposed in the literature, e.g., the correlation ratio [14], the Fourier amplitude sensitivity test indices [15] and the Sobol' indices [16]. Among these sensitivity measures, the Sobol' indices [16] have shown the largest accuracy in most cases and hence they will be incorporated in this study. Using the Sobol' indices, Abiatti et al. [17] evaluated the sensitivity of the probabilistic response of a structure due to the uncertainty of the structure and of the excitation parameters. Zeighami et al. [18] studied the Sobol' sensitivity of the stochastic mechanical behavior of a seismic meta-barrier with respect to its uncertain mechanical parameters. The Sobol' sensitivity analysis was also used for bridge retrofits in a regional road network subjected to an uncertain seismic hazard [19].

The Sobol' indices are commonly computed using the MCS. However, using the MCS, the evaluation of the Sobol' indices in the case of complex systems is computationally very demanding. To overcome the limitations of the MCS, the PC expansion [20–25] has been incorporated into the FEM. This enables efficient and accurate propagation and quantification of uncertainty. By combining the PC expansion and the FEM, the stochastic FEM (SFEM) has been developed [20, 26–31] and successfully applied in many engineering problems involving uncertainties, e.g., stochastic analysis of: fluid flow [23], seismic site response [10], shear frame structure [11,12] and earthquake soil-structure interacting system [32]. In addition, Sudret [33] developed Sobol' indices from the PC representation of probabilistic system response.

In this study, a novel numerical framework for the Sobol' sensitivity analysis of a 1D stochastic elasto-plastic seismic wave propagation is proposed and tested. The multi-dimensional Hermite PC expansion is used to represent both, the uncertain soil parameters and the uncertain bedrock motions. The probabilistic dynamic system response to the uncertain bedrock motions propagating through the uncertain elasto-plastic soil is obtained using the stochastic elasto-plastic FEM (SEPFEM) [30]. The Sobol' indices are computed from the PC-represented system response for the purpose of a global sensitivity analysis.

The main novelty of the presented framework relies on the combination and implementation of:

- an accurate modeling of uncertain seismic load using ground motion prediction equations of Fourier amplitude spectra and Fourier phase derivative [34,35]
- SEPFEM [30] based on the use of the PC expansion [10–12] and
- the Sobol' sensitivity analysis [16].

Such approach has not been proposed in the literature as yet. It has been implemented into Real-ESSI Simulator [36] and it is evaluated here.

## 2. Modeling of uncertain input, bedrock motions

Different ground motion prediction equations (GMPEs) have been proposed in the literature in order to estimate the variability of intensity measures of seismic motions, for example, the spectral acceleration, $Sa$, [37]. However, the variability of an intensity measure alone is not sufficient in a stochastic site response analysis. The quantification of uncertainty within a site response analysis requires the uncertain input time-domain seismic motions.

As proposed by Wang et al. [11,12], uncertain time-domain seismic motions can be inverse Fourier synthesized from the stochastic Fourier amplitude spectra (FAS) and Fourier phase spectrum (FPS). In this approach, the uncertain FAS of seismic motions is modeled as a log-normally distributed random process [34,35] in the frequency space, where the median behavior is quantified using the stochastic method by Boore [38] or the recently developed GMPEs of FAS by Bora et al. [39] and by Bayless and Abrahamson [40]. The inter-frequency correlation of the FAS random process should also be taken into account in the ground motion modeling [41]. Hence the recent inter-frequency correlation model for FAS [35,42] is adopted here.

The stochastic FPS complements the FAS in the modeling of uncertain motions. Boore [43] showed that the Fourier phase information of seismic motions can be obtained as the integral of the Fourier phase derivative $\dot{\Phi}$ defined as

$$\dot{\Phi} = \frac{\Delta\Phi}{\Delta f}, \tag{1}$$

where $\Delta\Phi$ is the Fourier phase difference within the frequency interval $\Delta f$. Based on 3551 recordings of ground motions from PEER NGA-West 1 database, Baglio [44] demonstrated that the distribution of the phase derivative, $\dot{\Phi}$, is leptokurtic and that it fits well to the logistic model. The GMPE for the logistic model parameter of the phase derivative [44] is applied in this study. Phase derivatives $\dot{\Phi}(f)$ for different frequencies are modeled as logistic distributed random fields described by the exponential correlation with correlation length $l_f = 0.05$ Hz.

Uncertain motions for seismic scenario with magnitude of the earthquake $M = 8$, distance from the source of the earthquake $R_{jb} = 12$ km and bedrock site condition $V_{s30} = 620$ m/s are simulated using the stochastic FAS and FPS. Currently available modeling of uncertain input, bedrock motions allows for the use of deterministic $V_{s30}$ only and hence, here, deterministic $V_{s30}$ is considered and used in GMPEs to compute FAS and FPS.

Here, 1500 realizations of the time-domain uncertain motions are generated. For example, in Fig. 1, three different realizations of the time-domain uncertain motions are plotted. Significant differences among these realizations can be observed, e.g. the peak ground acceleration (PGA) varies from 2.1 m/s$^2$ to 9.7 m/s$^2$.

The simulated motions should possess the desired uncertain characteristics that are consistent with the conventional GMPEs. Here, the generated uncertain motions are verified by comparison with the corresponding weighted average motions obtained from five different GMPEs from the NGA-West2 project [37] using weights 0.22 for ASK14, 0.22 for BSSA14, 0.22 for CB14, 0.22 for CY14 and 0.12 for I14. The weights for these five GMPEs are chosen based on work by Rezaeian et al. [45]. In Fig. 2, the spectral acceleration, $Sa$, of the simulated uncertain motions is plotted together with the one obtained from the GMPEs. The median $Sa$ from the simulated motions and the median $Sa$ obtained using the GMPEs coincide very well. It follows from Fig. 2(b) that the simulated motions also have the desired variability that is consistent with the variability term, i.e., the standard deviation, $\sigma$, obtained from the GMPEs. Using the GMPEs, the resulting distribution of the PGA is log-normal. In Fig. 3, a reasonable match between the simulated distribution of the PGA and the corresponding log-normal distribution of the PGA obtained from the GMPEs can be seen. Here, the uncertainty in PGA is obtained for a particular earthquake scenario, with $M = 8$ and $R_{jb} = 12$ km, and PDF of PGA does not account for different possible earthquake scenarios.

The distribution of the simulated accelerations at all time instances is observed to be Gaussian. Similar observations were made by Wang et al. [10] from the statistical analysis of a number of seismic recordings. The uncertain motions are modeled as a Gaussian distributed non-stationary random process and they are represented using the Hermite PC Karhunen-Loève (KL) expansion, as described in Section 3.

A random process incorporates much more information about the uncertain ground motions than the conventional GMPEs. The GMPEs only quantify the variability of a given intensity measure, for example, the spectral acceleration, $Sa$. Unlike the GMPEs, a random process contains information not only about the variability of a single intensity measure but also information about the variability of other important characteristics, e.g., PGA, peak ground velocity (PGV), Arias intensity, etc.

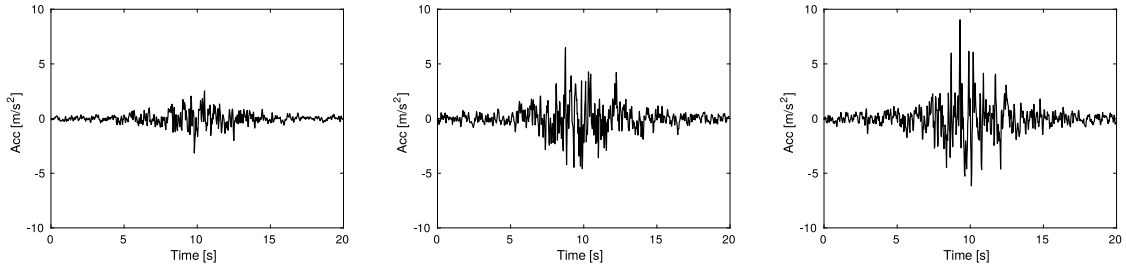


**Fig. 1.** Different realizations of the time-domain uncertain motions: acceleration (Acc) as function of time.

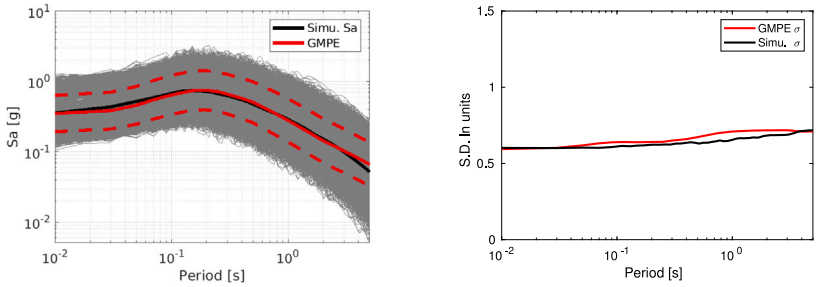


**(a)** Median **(b)** Standard deviation

**Fig. 2.** Verification of uncertain spectrum acceleration, $Sa$, of simulated motions against $Sa$ obtained from the GMPEs.

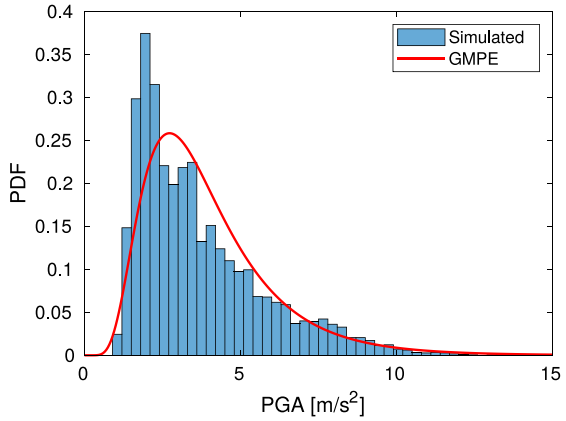


**Fig. 3.** Verification of the probability distribution function (PDF) of the simulated PGA against the PDF of the PGA obtained from the GMPEs.

## 3. Hermite Polynomial Chaos Karhunen-Loè ve Expansion

Hermite polynomial chaos (PC) Karhunen-Loève (KL) expansion will be used to discretize the general heterogeneous random field, $H(\boldsymbol{x},\theta)$, of an arbitrary probability distribution. Here, $\theta$ pertains to the random space and $\boldsymbol{x}$ is the general coordinate that can be either temporal, in the case of an uncertain random process, or spatial, in the case of an uncertain random field. Random field $H(\boldsymbol{x},\theta)$ with any type of the probability distribution can be discretized using the orthogonal Hermite PC, $\Omega_i(\gamma(\boldsymbol{x},\theta))$, up to a certain order, $P$, [20,21],

$$H(\boldsymbol{x},\theta) = \sum_{i=0}^{P} H_i(\boldsymbol{x})\Omega_i(\gamma(\boldsymbol{x},\theta))\,, \tag{2}$$

where random functions $\{\Omega_i(\gamma)\}$ are Hermite polynomials constructed from zero mean, unit variance Gaussian random field $\gamma(\boldsymbol{x},\theta)$. These random functions $\{\Omega_i(\gamma)\}$ are determined from the initial condition $\Omega_0 = 1$ and the recursive relation [20,21],

$$\Omega_{i+1}(\gamma) = \gamma\Omega_i(\gamma) - \Omega_i'(\gamma)\,. \tag{3}$$

The deterministic PC coefficient field, $H_i(\boldsymbol{x})$, can be calculated by projecting random field $H(\boldsymbol{x},\theta)$ onto the PC basis $\{\Omega_i\}$. Given the input covariance, $C_H(x_1,x_2)$, of the original random field, the covariance, $C_\gamma(x_1,x_2)$, of Gaussian random field $\gamma(\boldsymbol{x},\theta)$ can be determined from

$$C_H(x_1,x_2) = \sum_{i=1}^{P} H_i(x_1)\; H_i(x_2)\; i\,!\; C_\gamma(x_1,x_2)^i\,, \tag{4}$$

see [21]. Using the KL expansion [20], the underlying Gaussian random field, $\gamma(\boldsymbol{x},\theta)$, can be represented as

$$\gamma(\boldsymbol{x},\theta) = \sum_{i=1}^{M} \sqrt{\lambda_i} f_i(\boldsymbol{x})\xi_i(\theta)\,, \tag{5}$$

where the eigenvalues, $\lambda_i$, and eigenfunctions, $f_i(\boldsymbol{x})$, of covariance $C_\gamma(x_1,x_2)$ have to satisfy the Fredholm's integral equation of the second kind [21]. Zero mean and unit variance Gaussian random variables $\{\xi_i(\theta)\}$ are represented in $M$ independent dimensions.

By combining Eqs. (2) to (5), the PC-KL expansion of random field $H(\boldsymbol{x},\theta)$ into multi-dimensional orthogonal Hermite PC basis $\{\Psi_i\}$ of order $P$ and dimension $M$ can be obtained as

$$H(\boldsymbol{x},\theta) = \sum_{i=0}^{K} h_i(\boldsymbol{x})\Psi_i(\{\xi_j(\theta)\}) \tag{6}$$

$$h_i(\boldsymbol{x}) = \frac{p!}{\langle\Psi_i^2\rangle} H_p(\boldsymbol{x}) \prod_{j=1}^{p} \frac{\sqrt{\lambda_{k(j)}} f_{k(j)}(\boldsymbol{x})}{\sqrt{\sum_{m=1}^{M}(\sqrt{\lambda_m} f_m(\boldsymbol{x}))^2}}\,, \tag{7}$$

where $K$ is the maximum order of the multi-dimensional Hermite PC basis $\{\Psi_i\}$ that depends on order $P$ and dimension $M$, i.e., $K = 1 + \sum_{s=1}^{P} \frac{1}{s!}\prod_{j=0}^{s-1}(M+j)$. The upper product limit $p$, in Eq. (7) is the order of $\Psi_i(\{\xi_j(\theta)\})$. The mean, variance, correlation and any other statistics of random field $H(\boldsymbol{x},\theta)$ can be obtained from the above Hermite PC-KL expansion. The accuracy of the PC-KL expansion can be evaluated by comparing the statistics obtained from the PC-KL expansion with the input statistics of random field $H(\boldsymbol{x},\theta)$.

## 4. Galerkin stochastic elasto-plastic finite element method

The uncertain material properties and the uncertain input motions are modeled in Section 6 as heterogeneous random fields and

a non-stationary random process, respectively. The Hermite PC expansion is applied to both, the input uncertainties and the output uncertainties, like the probabilistic displacement or acceleration fields. The stochastic Galerkin projection is used in order to minimize the error in the PC coefficients of the output fields. These PC coefficients are used to obtain the statistics and distributions of the uncertain output fields.

The weak form of the deterministic discrete dynamic equilibrium equation [46] can be written as

$$\int_{D_e} N_m(\boldsymbol{x})\rho(\boldsymbol{x})N_n(\boldsymbol{x})dV\ \ddot{u}_n(t) + \int_{D_e} \nabla N_m(\boldsymbol{x})E(\boldsymbol{x})\nabla N_n(\boldsymbol{x})dV\ u_n(t) - f_m(t) = 0\,, \tag{8}$$

where $N_m(\boldsymbol{x}), N_n(\boldsymbol{x})$ are the shape functions, $f_m(t)$ is the nodal force, $\rho(\boldsymbol{x})$ is the deterministic material density and $E(\boldsymbol{x})$ is the deterministic, elastic or elasto-plastic, material stiffness.

The tangent stiffness, $E(\boldsymbol{x})$, is generally a heterogeneous random field and the dynamic nodal force, $f_m(t)$, is a non-stationary random process. Both, $E(\boldsymbol{x})$ and $f_m(t)$, can be represented using multi-dimensional Hermite PC expansions

$$E(\boldsymbol{x},\theta) = \sum_{i=0}^{P_1} E_i(\boldsymbol{x})\Psi_i(\{\xi_r(\theta)\}) \tag{9}$$

$$f_m(t,\theta) = \sum_{j=0}^{P_2} f_{mj}(t)\psi_j(\{\xi_r(\theta)\}) \tag{10}$$

with known PC coefficients, $E_i(\boldsymbol{x})$ and $f_{mj}(t)$.

When a system with uncertain properties is excited by uncertain loads, the resulting displacement and acceleration are also uncertain and they can be represented using the Hermite PC expansions up to order $P_3$,

$$u_n(t,\theta) = \sum_{k=0}^{P_3} u_{nk}(t)\phi_k(\{\xi_l(\theta)\}) \tag{11}$$

$$\ddot{u}_n(t,\theta) = \sum_{k=0}^{P_3} \ddot{u}_{nk}(t)\phi_k(\{\xi_l(\theta)\})\,, \tag{12}$$

with unknown PC coefficients $u_{nk}(t)$ and $\ddot{u}_{nk}(t)$.

After substituting Eqs. (9) to (12) into Eq. (8), and denoting the gradient, $\nabla N_n(\boldsymbol{x})$, of a shape function, $N_n(\boldsymbol{x})$, as $B_n(\boldsymbol{x})$, one arrives at

$$\sum_{k=0}^{P_3}\int_{D_e} N_m(\boldsymbol{x})\rho(\boldsymbol{x})N_n(\boldsymbol{x})dV\ \phi_k\ddot{u}_{nk}(t)\ + \sum_{k=0}^{P_3}\sum_{i=0}^{P_1}\int_{D_e} B_m(\boldsymbol{x})E_i(\boldsymbol{x})B_n(\boldsymbol{x})dV\ \Psi_i\phi_k u_{nk}(t) - \sum_{j=0}^{P_2} f_{mj}(t)\psi_j = 0\,. \tag{13}$$

Eq. (13) can be multiplied with PC basis $\phi_l$ [26] and, then, the expectation operator, $\langle\cdot\rangle$, can be applied to obtain

$$\sum_{k=0}^{P_3}\langle\phi_k\phi_l\rangle\int_{D_e} N_m(\boldsymbol{x})\rho(\boldsymbol{x})N_n(\boldsymbol{x})dV\ \ddot{u}_{nk}(t)\ + \sum_{k=0}^{P_3}\sum_{i=0}^{P_1}\langle\Psi_i\phi_k\phi_l\rangle\int_{D_e} B_m(\boldsymbol{x})E_i(\boldsymbol{x})B_n(\boldsymbol{x})dV\ u_{nk}(t) = \sum_{j=0}^{P_2}\langle\psi_j\phi_l\rangle f_{mj}(t) \tag{14}$$

with $l = 0,1,2,\ldots,P_3$, where $P_3$ is the maximum order of the PC expansion, $m = 1,2,\ldots,N$ and $N$ is the number of FE nodes. Eq. (14) represents the stochastic Galerkin projection. The expectations of double products, $\langle\phi_k\phi_l\rangle$, $\langle\psi_j\phi_l\rangle$, and of triple products, $\langle\Psi_i\phi_k\phi_l\rangle$, can be analytically computed beforehand and used in the SEPFE calculation.

Eq. (14) can be rewritten into the following tensor form

$$\boldsymbol{M}:\ddot{\boldsymbol{u}} + \boldsymbol{K}:\boldsymbol{u} = \boldsymbol{F}\,, \tag{15}$$

where $\boldsymbol{M}$, $\boldsymbol{K}$ and $\boldsymbol{F}$ are the stochastic mass, stiffness and force, respectively. The unknown PC coefficients of the acceleration and displacement are denoted as $\ddot{\boldsymbol{u}}$ and $\boldsymbol{u}$, respectively.

Eq. (15) can be further rewritten using the index notation with the Einstein summation convention,

$$M_{mlnk}\ddot{u}_{nk} + K_{mlnk}u_{nk} = F_{ml}\,, \tag{16}$$

where the following holds

$$M_{mlnk} = \bigcup_e \langle\phi_k\phi_l\rangle\int_{D_e} N_m(\boldsymbol{x})\rho(\boldsymbol{x})N_n(\boldsymbol{x})dV \tag{17}$$

$$K_{mlnk} = \bigcup_e \sum_{i=0}^{P_1}\langle\Psi_i\phi_k\phi_l\rangle\int_{D_e} B_m(\boldsymbol{x})E_i(\boldsymbol{x})B_n(\boldsymbol{x})dV \tag{18}$$

$$F_{ml} = \bigcup_e \sum_{j=0}^{P_2}\langle\psi_j\phi_l\rangle f_{mj} \tag{19}$$

and $\bigcup_e$ is the assembly operator for the elemental mass, stiffness and force. The Rayleigh damping can also be taken into account, that is,

$$\boldsymbol{M}:\ddot{\boldsymbol{u}} + \boldsymbol{C}:\dot{\boldsymbol{u}} + \boldsymbol{K}:\boldsymbol{u} = \boldsymbol{F}\,. \tag{20}$$

The stochastic damping matrix is

$$\boldsymbol{C} = \alpha\boldsymbol{M} + \beta\boldsymbol{K}\,, \tag{21}$$

where $\alpha$ and $\beta$ are the Rayleigh damping parameters. The Rayleigh damping corresponds to the damping ratio, $\xi$, being a function,

$$\xi = \frac{1}{2}\left(\frac{\alpha}{\omega} + \beta\omega\right), \tag{22}$$

of the response frequency, $\omega$, see Chopra [47]. The uncertainty in the Rayleigh damping is included via the uncertainties of the mass and stiffness. In Eq. (21), both, mass $\boldsymbol{M}$ and stiffness $\boldsymbol{K}$, are stochastic and account for the uncertainties from the material density and stiffness. Additional uncertainties could be included through the uncertain Rayleigh damping parameters, $\alpha$ and $\beta$. However, these uncertainties are difficult to quantify. Hence, in this study, Rayleigh parameters, $\alpha$ and $\beta$, are assumed to be deterministic and the uncertainty in the damping results solely from the uncertainty in the mass and stiffness. The same Galerkin projection scheme as in Eq. (14) is applied to propagate the uncertainty from the damping through the system.

Eqs. (15) and (20) can be solved using, for example, the Newmark time integration method [48]. The size of the SEPFE system of equations is larger compared to the corresponding deterministic FE system of equations. This difference results from the PC expansion used to represent the probabilistic displacement and acceleration fields.

After solving Eq. (15) or (20) for the unknown PC coefficients of the displacement, $u_{nk}$, and of the acceleration, $\ddot{u}_{nk}$, one obtains the complete probabilistic dynamic response of the system. Using these PC coefficients, $u_{nk}$ and $\ddot{u}_{nk}$, any probabilistic characteristic of the uncertain system response can be obtained. For example, the time-evolving mean and variance of the probabilistic displacement response at node $n$ can be computed as follows

$$\langle u_n(t,\theta)\rangle = u_{n0}(t) \tag{23}$$

$$\mathrm{Var}(u_n(t,\theta)) = \sum_{k=1}^{P_3}\langle\phi_k^2\rangle u_{nk}^2(t)\,. \tag{24}$$

### 4.1. Probabilistic elasto-plastic constitutive modeling

The probabilistic 1D tangent stiffness, $E(\boldsymbol{x},\theta)$, needs to be updated at each incremental step. The probabilistic elasto-plastic constitutive model is called at each Gauss point to update the uncertain elasto-plastic stiffness and stress. The constitutive behavior of the soil is described by a 1D elasto-plastic material model with a vanishing elastic region and the Armstrong-Frederick non-linear kinematic hardening [49,50].

The 1D deterministic relationship between the stress increment, $\mathrm{d}\sigma$, and the strain increment $\mathrm{d}\epsilon$, can be written as

$$\mathrm{d}\sigma = H_a\mathrm{d}\epsilon - C_r\sigma|\mathrm{d}\epsilon|\,, \tag{25}$$

where $H_a$ and $C_r$ are the model parameters [49,50]. The resulting shear strength is $S_u = H_a/C_r$. The elasto-plastic tangent stiffness is a function of stress $\sigma$,

$$E(\sigma) = \frac{d\sigma}{\mathrm{d}\epsilon} = H_a - C_r\sigma\ \mathrm{sgn}(\mathrm{d}\epsilon)\,, \tag{26}$$

where sgn(d$\epsilon$) is the sign function of the strain increment, d$\epsilon$. This function returns sgn(d$\epsilon$) = 1 for d$\epsilon > 0$ and sgn(d$\epsilon$) = −1 otherwise.

Here, the model parameters, $H_a$ and $C_r$, are uncertain and they are represented as random fields using the Hermite PC expansion with basis $\{\varphi_i(\{\xi_r(\theta)\})\}$, i.e.,

$$H_a(\boldsymbol{x},\theta) = \sum_{i=0}^{P} H_{ai}(\boldsymbol{x})\varphi_i(\{\xi_r(\theta)\}) \tag{27}$$

$$C_r(\boldsymbol{x},\theta) = \sum_{i=0}^{P} C_{ri}(\boldsymbol{x})\varphi_i(\{\xi_r(\theta)\})\,. \tag{28}$$

Strain increments $\mathrm{d}\epsilon(\boldsymbol{x},\theta)$ represent input to the constitutive driver, see Eq. (25). Strain increments $\mathrm{d}\epsilon(\boldsymbol{x},\theta)$ are also uncertain and are obtained from displacements using $\epsilon(\boldsymbol{x},\theta) = B(\boldsymbol{x})u_n(t,\theta)$, so that

$$\mathrm{d}\epsilon(\boldsymbol{x},\theta) = \sum_{i=0}^{P} \mathrm{d}\epsilon_i(\boldsymbol{x})\varphi_i(\{\xi_r(\theta)\})\,. \tag{29}$$

The probabilistic incremental stress, $\mathrm{d}\sigma(\boldsymbol{x},\theta)$, and the tangent stiffness, $E(\boldsymbol{x},\theta)$, can be represented using unknown PC coefficients $\mathrm{d}\sigma_i(\boldsymbol{x})$ and $E_i(\boldsymbol{x})$,

$$\mathrm{d}\sigma(\boldsymbol{x},\theta) = \sum_{i=0}^{P} \mathrm{d}\sigma_i(\boldsymbol{x})\varphi_i(\{\xi_r(\theta)\}) \tag{30}$$

$$E(\boldsymbol{x},\theta) = \sum_{i=0}^{P} E_i(\boldsymbol{x})\varphi_i(\{\xi_r(\theta)\})\,. \tag{31}$$

Eqs. (27) to (31) can be substituted into Eqs. (25) and (26). Then, both equations can be multiplied with PC basis $\varphi_m$ and the expectation operator, $\langle\cdot\rangle$, can be applied to obtain

$$\sum_{i=0}^{P} \mathrm{d}\sigma_i\langle\varphi_m\varphi_i\rangle = \sum_{i=0}^{P}\sum_{k=0}^{P} H_{ai}\mathrm{d}\epsilon_k\langle\varphi_m\varphi_k\varphi_i\rangle \pm \sum_{i=0}^{P}\sum_{n=0}^{P}\sum_{s=0}^{P} C_{ri}\sigma_n\mathrm{d}\epsilon_s\langle\varphi_m\varphi_n\varphi_s\varphi_i\rangle \tag{32}$$

$$\sum_{i=0}^{P} E_i\langle\varphi_m\varphi_i\rangle = \sum_{i=0}^{P} H_{ai}\langle\varphi_m\varphi_i\rangle \pm \sum_{i=0}^{P}\sum_{n=0}^{P} C_{ri}\sigma_n\langle\varphi_m\varphi_n\varphi_i\rangle\,. \tag{33}$$

Unknown PC coefficients of the incremental stress $\mathrm{d}\sigma_i(\boldsymbol{x})$ and of the elasto-plastic stiffness $E_i(\boldsymbol{x})$ can be computed using the orthogonality of the Hermite PC basis,

$$\mathrm{d}\sigma_i = \frac{1}{\mathrm{Var}[\varphi_i]}\left[H_{aj}\mathrm{d}\epsilon_k\langle\varphi_j\varphi_k\varphi_i\rangle \pm C_{rl}\sigma_n\mathrm{d}\epsilon_s\langle\varphi_l\varphi_n\varphi_s\varphi_i\rangle\right] \tag{34}$$

$$E_i = H_{ai} \pm \frac{1}{\mathrm{Var}[\varphi_i]}C_{rl}\sigma_n\langle\varphi_l\varphi_n\varphi_i\rangle\,, \tag{35}$$

where $\mathrm{Var}[\varphi_i]$ is the variance of $\varphi_i\{\xi_r(\theta)\}$ and it equals to $\langle\varphi_i^2\rangle$. The Einstein's summation convention is used in Eqs. (34) and (35) with index $i$ being a free index. The probabilistic material response, d$\sigma$, is here obtained using the explicit forward Euler algorithm [46].

In Fig. 4, the stress-strain relation is plotted using the uncertain material parameters, representing initial stiffness, $H_a$ with the mean of 10 MPa and the coefficient of variation, CV = 25%, and the uncertain shear strength, $S_u = H_a/C_r$, with the mean of 150 kPa and CV = 25%. The material is driven by uncertain cyclic strain with the mean strain increment of $10^{-4}$ and CV = 20%.

The SEPFE material response matches well the MCS with 10,000 samples. The SEPFE is nearly 2000 times more computationally efficient than the MCS, for the same level of accuracy.

## 5. Sobol' sensitivity analysis using the polynomial chaos expansion

In the Sobol' sensitivity analysis, the variance of the uncertain output of a model is decomposed into the sum of contributions from the individual random inputs and groups of random inputs. A mathematical model with $n$ uncertain independent inputs gathered in vector $\boldsymbol{x}$ and the resulting uncertain scalar output,

$$y = f(\boldsymbol{x})\,, \tag{36}$$

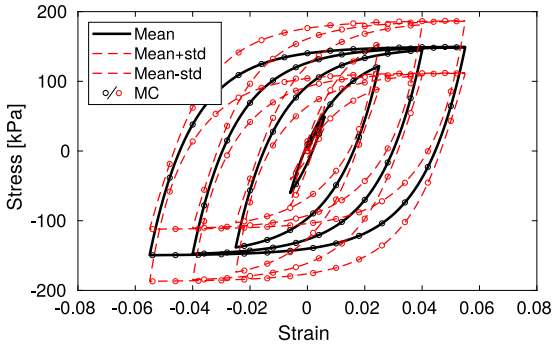


**Fig. 4.** Hysteretic behavior of 1D elasto-plastic material with uncertain parameters $H_a$ and $S_u = H_a/C_r$.

is considered. This uncertain scalar $y$ is assumed to have a finite variance. Model output $f(\boldsymbol{x})$ can be decomposed [16] in the following way

$$f(x_1,x_2,\ldots,x_n) = f_0 + \sum_{i=1}^{n} f_i(x_i) + \sum_{1\le i<j\le n} f_{ij}(x_i,x_j) + \cdots + f_{1,2,\ldots,n}(x_1,\ldots,x_n)\,. \tag{37}$$

Eq. (37) is known as the analysis of variance (ANOVA) representation of $f(\boldsymbol{x})$. There are $2^n$ summands in Eq. (37). Constant $f_0$ is the mean value of $f(\boldsymbol{x})$. The integral of each summand in Eq. (37) over any of its independent random arguments is zero,

$$\int f_{i_1,\ldots,i_s}(x_{i_1},x_{i_2},\ldots,x_{i_s})\,\mathrm{d}x_{i_k} = 0 \quad \text{for} \quad 1\le k\le s\le n\,. \tag{38}$$

Using Eq. (38), it can be shown that the summands are orthogonal to each other, i.e.,

$$\int f_{i_1,\ldots,i_s}(x_{i_1},x_{i_2},\ldots,x_{i_s})f_{j_1,\ldots,j_t}(x_{j_1},x_{j_2},\ldots,x_{j_t})\,\mathrm{d}\boldsymbol{x} = 0 \quad \text{for} \quad \{i_1,\ldots,i_s\}\neq\{j_1,..,j_t\}\,. \tag{39}$$

For given mathematical model $f(\boldsymbol{x})$, the above ANOVA representation, Eq. (37), is unique and can be derived analytically. The univariate terms can be found as

$$f_i(x_i) = \int f(\boldsymbol{x})\,d\boldsymbol{x}_{\sim i} - f_0\,, \tag{40}$$

where $\int(\cdot)\,d\boldsymbol{x}_{\sim i}$ denotes the integration over all dimensions except $x_i$. Similarly, the bivariate terms can be derived as

$$f_{ij}(x_i,x_j) = \int f(\boldsymbol{x})\,d\boldsymbol{x}_{\sim[ij]} - f_i(x_i) - f_j(x_j) - f_0\,. \tag{41}$$

Any summand, $f_{i_1,\ldots,i_s}(x_{i_1},x_{i_2},\ldots,x_{i_s})$, in Eq. (37) can be obtained using multidimensional integrals of model output $f(\boldsymbol{x})$.

The total variance of the probabilistic model response, $y = f(\boldsymbol{x})$, is

$$D = \mathrm{Var}[f(\boldsymbol{x})] = \int f^2(\boldsymbol{x})\,d\boldsymbol{x} - f_0^2\,. \tag{42}$$

Using Eqs. (37) and (39), the total variance, $D$, can be decomposed as follows

$$D = \sum_{i=1}^{n} D_i + \sum_{1\le i<j\le n} D_{ij} + \cdots + D_{1,2,\ldots,n}\,. \tag{43}$$

The individual summands in Eq. (43) are given by

$$D_{i_1,\ldots,i_s} = \int f^2_{i_1,\ldots,i_s}(x_{i_1},\ldots,x_{i_s})\,\mathrm{d}x_{i_1},\ldots,\mathrm{d}x_{i_s} \text{ with } 1\le i_1<\cdots<i_s\le n,\quad s=1,\ldots,n\,. \tag{44}$$

The Sobol' indices are defined as

$$S_{i_1,\ldots,i_s} = D_{i_1,\ldots,i_s}/D\,. \tag{45}$$

The Sobol' indices, $S_{i_1,\dots,i_s}$, express the fractional contributions from independent random inputs stored as $\boldsymbol{x} = \{x_{i_1},\dots,x_{i_s}\}$ to the total variance, $D$. The first order indices, $S_i$, describe the individual influence of each uncertain input, $x_i$. The higher-order terms describe the mixed influence, when a group of uncertain inputs is considered. From Eq. (43), it follows that

$$\sum_{i=1}^{n} S_i + \sum_{1\le i<j\le n} S_{i,j} + \cdots + S_{1,2,\dots,n} = 1\,. \tag{46}$$

The total sensitivity index, $S_i^{\text{total}}$, is defined to evaluate the total influence of a given input, $x_i$, as

$$S_i^{\text{total}} = \sum_{\mathscr{S}_i} D_{i_1,\dots,i_s}\,, \tag{47}$$

where set $\mathscr{S}_i$ gathers all $i_1,\dots,i_s$ that include $i$,

$$\mathscr{S}_i = \{(i_1,\dots,i_s) : \exists k, 1\le k\le s, i_k = i\}\,. \tag{48}$$

Sobol' indices $D_{i_1,\dots,i_s}$ in Eq. (47) are partial sensitivity indices related to a given input, $x_i$.

Using the Hermite PC expansion [20], the probabilistic model response, $y = f(\boldsymbol{x})$, can be represented as

$$y = \sum_{j=0}^{P} y_j \Psi_j(\boldsymbol{\xi}), \quad \boldsymbol{\xi} = \{\xi_1,\dots,\xi_M\}\,, \tag{49}$$

where $\{\Psi_j\}$ is multi-dimensional orthogonal Hermite PC basis of maximum order $P$ that is constructed from $M$-dimensional standard Gaussian random vector $\boldsymbol{\xi}$ with independent components $\xi_i$.

The input random vector, $\boldsymbol{x}$, of any prescribed joint PDF or any given marginal PDF and correlation can be approximately transformed into the standard Gaussian random vector, $\boldsymbol{\xi}$, using a transformation technique, for example, the isoprobabilistic transform and the Nataf transform [51]. Therefore, the probabilistic model response can be evaluated and represented using the Hermite PC expansion from Eq. (49). Here, the input random vector, $\boldsymbol{x}$, is transformed into the standard Gaussian random vector, $\boldsymbol{\xi}$, and the Hermite PC expansion is used. The input random vector, $\boldsymbol{x}$, can also be transformed into other standard random variables, e.g. into the standard uniform random variable, and the model response, $y$, can, then, be represented using the PC expansion [22].

The PC basis, $\{\Psi_j(\boldsymbol{\xi})\}$, is zero mean and orthogonal. Hence the mean, $\bar{y}$, and the total variance of the model response, $D^{PC}$, can be calculated from its PC representation,

$$\begin{aligned} \bar{y} &= \boldsymbol{E}[f(\boldsymbol{x})] = y_0 \\ D^{PC} &= \text{Var}\left[\sum_{j=0}^{P} y_j\Psi_j\right] = \sum_{j=1}^{P} y_j^2 \boldsymbol{E}\left[\Psi_j^2\right]\,, \end{aligned} \tag{50}$$

where $\boldsymbol{E}[\cdot]$ is the expectation operator.

To compute the Sobol' indices, the PC expansion of the model response, $y$, from Eq. (49) needs to be reorganized into the ANOVA form [33]. The multi-dimensional PC basis, $\{\Psi_j(\boldsymbol{\xi})\}$, is generally obtained as the tensor product of uni-dimensional PC bases,

$$\Psi_j(\boldsymbol{\xi}) = \prod_{i=1}^{n} \phi_{\alpha_i}(\xi_i)\,, \tag{51}$$

where $\phi_{\alpha_i}(\xi_i)$ is a uni-dimensional polynomial of order $\alpha_i$ in $\xi_i$. This $\phi_{\alpha_i}(\xi_i)$ is dependent on the standard random variable, $\xi_i$, [22]. The connection between the PC expansion of model response $y$ from Eq. (49), and the ANOVA representation of $y$ from Eq. (36) can be established by defining set $\mathscr{S}$ from $\boldsymbol{\alpha}$ as [33]

$$\begin{aligned} \mathscr{S}_{i_1,\dots,i_s} = \big\{\boldsymbol{\alpha} : \forall k = 1,\dots,n, \text{when } k\in(i_1,\dots,i_s),\ \alpha_k > 0,\ \text{otherwise,} \\ \alpha_k = 0\big\}\,. \end{aligned} \tag{52}$$

For example, set $\mathscr{S}_i$ would correspond to the PC basis depending only on dimension $\xi_i$. With Eq. (52), the PC expansion from Eq. (49) can be rewritten into the ANOVA representation as

$$\begin{aligned} y = y_0 &+ \sum_{i=1}^{n}\sum_{\boldsymbol{\alpha}\in\mathscr{S}_i} y_{\boldsymbol{\alpha}}\Psi_{\boldsymbol{\alpha}}(\xi_i) + \sum_{1\le i_1<i_2\le n}\sum_{\boldsymbol{\alpha}\in\mathscr{S}_{i_1,i_2}} y_{\boldsymbol{\alpha}}\Psi_{\boldsymbol{\alpha}}(\xi_{i_1},\xi_{i_2}) + \cdots \\ &+ \sum_{1\le i_1<\cdots<i_s\le n}\sum_{\boldsymbol{\alpha}\in\mathscr{S}_{i_1,\dots,i_s}} y_{\boldsymbol{\alpha}}\Psi_{\boldsymbol{\alpha}}(\xi_{i_1},\dots,\xi_{i_s}) + \cdots \\ &+ \sum_{\boldsymbol{\alpha}\in\mathscr{S}_{1,2,\dots,n}} y_{\boldsymbol{\alpha}}\Psi_{\boldsymbol{\alpha}}(\xi_1,\dots,\xi_n)\,, \end{aligned} \tag{53}$$

where the term $\sum_{\boldsymbol{\alpha}\in\mathscr{S}_{i_1,\dots,i_s}} y_{\boldsymbol{\alpha}}\Psi_{\boldsymbol{\alpha}}(\xi_{i_1},\dots,\xi_{i_s})$ denotes the summation of these PC expansions which depend on standard random variables $\{\xi_{i_1},\dots,\xi_{i_s}\}$ only. Using Eq. (53), the PC-based Sobol' indices can be derived as

$$S^{PC}_{i_1,\dots,i_s} = \sum_{\boldsymbol{\alpha}\in\mathscr{S}_{i_1,\dots,i_s}} y_{\boldsymbol{\alpha}}^2 \boldsymbol{E}\left[\Psi_{\boldsymbol{\alpha}}^2\right]/D^{PC}\,. \tag{54}$$

The total Sobol' indices, $S^{PC,\text{total}}_{j_1,\dots,j_t}$, for any group of random inputs can be obtained as

$$S^{PC,\text{total}}_{j_1,\dots,j_t} = \sum_{(i_1,\dots,i_s)\in\mathscr{S}_{j_1,\dots,j_t}} S^{PC}_{i_1,\dots,i_s}\,, \tag{55}$$

where set $\mathscr{S}_{j_1,\dots,j_t}$ is defined as

$$\mathscr{S}_{j_1,\dots,j_t} = \{(i_1,\dots,i_s) : (j_1,\dots,j_t)\subset(i_1,\dots,i_s)\}\,. \tag{56}$$

Once the PC representation of the probabilistic model response is established, the Sobol' sensitivity indices can be analytically evaluated with a very small computational cost.

## 6. Sobol' sensitivity analysis of a 1D elasto-plastic shear wave propagation

### 6.1. Uncertain soil properties

Let us consider the stochastic site response of a 10 m soil layer described by uncertain material properties and subjected to uncertain bedrock motions. The soil is discretized into 10 shear beam elements with the size of 1 m, Fig. 5. The soil is modeled using 1D elasto-plastic material with a vanishing elastic region and the Armstrong-Frederick kinematic hardening from Section 4.1. Solely the uncertainty in material parameter $H_a$, being the initial stiffness, i.e., the stiffness at the geostatic stress state, is taken into account. Material parameter $C_r$ is assumed to be deterministic, due to the practical difficulties in the estimation of its statistical properties. To ensure positive initial stiffness, $H_a$ is represented as log-normally distributed random field with the mean of 10 MPa and CV = 25%. Parameter $C_r$ is taken as 55.6. The uncertainty in the strength parameter, $S_u = H_a/C_r$, with the mean of 180 kPa and CV = 25% [2,52] is due to the uncertainty in $H_a$. The correlation of material parameter $H_a$ is modeled as exponential

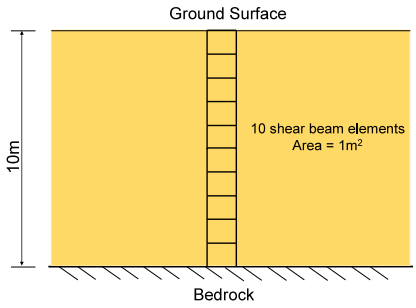


**Fig. 5.** 1D shear beam model.

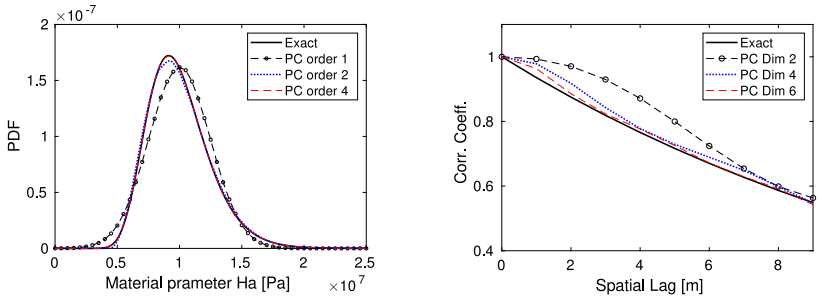


**(a)** PDF **(b)** Auto-correlation

**Fig. 6.** Uncertainty characterization of random field $H_a(\boldsymbol{x}, \theta)$.

function with correlation length $l_c = 15$ m as per Eq. (57). The correlation of the strength parameter, $S_u = H_a/C_r$, is the same as the one of material parameter $H_a$.

$$\rho(x_1, x_2) = e^{-\frac{|x_1 - x_2|}{l_c}} \tag{57}$$

Unit weight $\gamma = 18$ kN/m$^3$ of the soil is deterministic. The Rayleigh damping is used with deterministic parameters, $\alpha = 0.7$ Hz and $\beta = 4.2 \times 10^{-3}$ s. Parameters $\alpha$ and $\beta$ are selected to obtain damping ratio $\xi \approx 7\%$, see Argyris and Mlejnek [53], over frequencies of interest, i.e., 1...10 Hz, cf. Eq. (22). The uncertain material parameters are represented using the Hermite PC-KL expansion, see Section 3. The PC with order 2 captures the log-normal distribution of material parameter $H_a$ and it is computationally more efficient than the PC of order 4, see Fig. 6(a). The PC of dimension 4 is sufficient for the input exponential correlation of material parameter $H_a$, see Fig. 6(b). Therefore, the Hermite PC expansion of dimension 4 and order 2 is used for the PC representation of uncertain material parameters.

### 6.2. Uncertain input motions

Input, bedrock motions are another source of the uncertainty. The stochastic motions from Section 2 correspond to seismic scenario with magnitude of the earthquake $M = 8$, distance from the source of the earthquake $R_{jb} = 12$ km and bedrock site condition $V_{s30} = 620$ m/s and they are used here. These uncertain input motions are modeled as a non-stationary random process with statistics, e.g., mean, standard deviation and correlation structure, obtained from 1500 simulated realizations of uncertain motions from Section 2. As shown in Fig. 7, the mean of this random process is close to zero and is much smaller compared to the standard deviation.

The probability distribution of the random process is Gaussian and hence the Hermite PC expansion with order 1 is sufficient, as shown in Fig. 7. The statistics synthesized from the PC representation are exact, see Fig. 7. However, a relatively large-dimensional Hermite PC expansion is required to capture the non-stationary correlation of the random process, see Fig. 8(a). The Hermite PC expansions with order 1 and different values of dimension, namely, 50, 100 and 200 are tested. It is found that 50 dimensions of the Hermite PC expansion do not suffice to capture the correlation of the random process, see Table 1. The use of a larger-dimensional PC expansion allows to capture the correlation better. However, large dimensional PC expansion will also increase the computational cost of the SEPFE analysis. In Table 1, the errors in the mean, standard deviation and correlation for different dimensions of the PC expansion are given. Here, the ground motions will be represented as a non-stationary random process with the PC expansion of order 1 and dimension 100. The choice of the order and dimension is dictated by the optimal accuracy and computational efficiency.

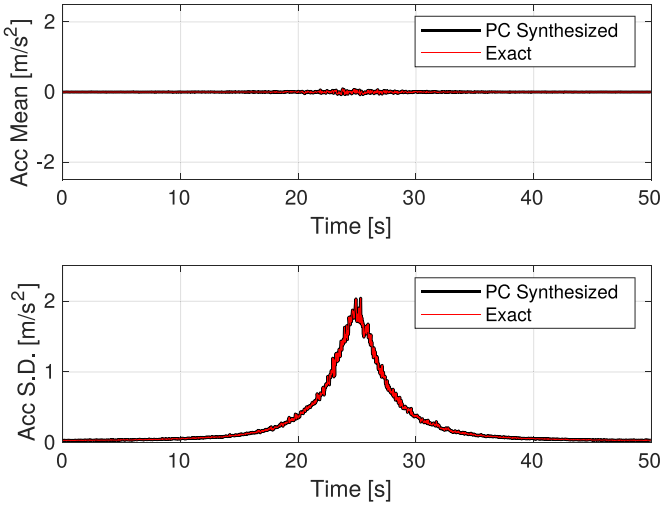


**Fig. 7.** Verification of the mean and standard deviation of the Hermite PC-KL expansion of the uncertain motions.

**Table 1**
Errors in the mean, standard deviation (S.D.) and correlation of the Hermite PC-KL expansion of the uncertain motions.

| PC dimension | Dim. 50 | Dim. 100 | Dim. 200 |
|---|---|---|---|
| Mean error [m/s$^2$] | $1.74 \times 10^{-11}$ | $1.74 \times 10^{-11}$ | $1.74 \times 10^{-11}$ |
| S.D. error [m/s$^2$] | $2.06 \times 10^{-9}$ | $2.06 \times 10^{-9}$ | $2.06 \times 10^{-9}$ |
| Correlation error | 0.11 | 0.039 | 0.014 |

### 6.3. Probabilistic elasto-plastic wave propagation

After both, the uncertain material parameters and the uncertain input motions, are discretized using the Hermite PC-KL expansion, the stochastic elasto-plastic seismic wave propagation can be analyzed using the SEPFEM. Here, its implementation in Real-ESSI Simulator [36] was used. The Hermite PC expansion of dimension 4 is used for the uncertain material parameters and the Hermite PC expansion of dimension 100 is used for the uncertain seismic motions. Hence the dimension of the Hermite PC expansion of the resulting fields, e.g., displacement or acceleration, is 104.

In a single SEPFE calculation, the complete probabilistic site response is obtained from the intrusive propagation of the uncertain input motions through the uncertain material. It is more computationally efficient compared to the conventional Monte Carlo approach. The presented case study took less than 15 min on a 4-core machine with 16 GB memory. The time-evolving mean and standard deviation of displacement and acceleration at the ground surface and at the depth of 5 m are plotted in Figs. 9 and 10.

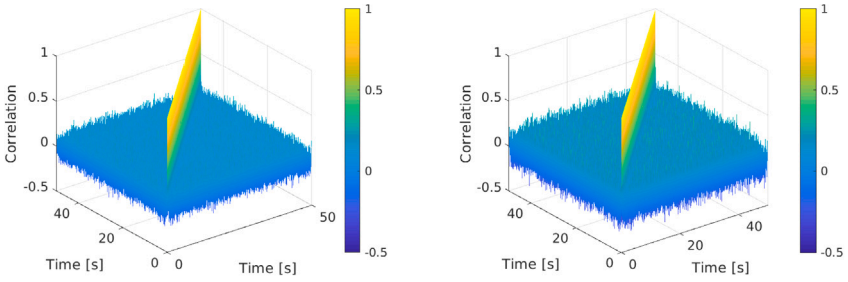


**(a)** Exact **(b)** PC with Dim. 100

**Fig. 8.** Verification of the correlation of the Hermite PC-KL expansion of uncertain motions.

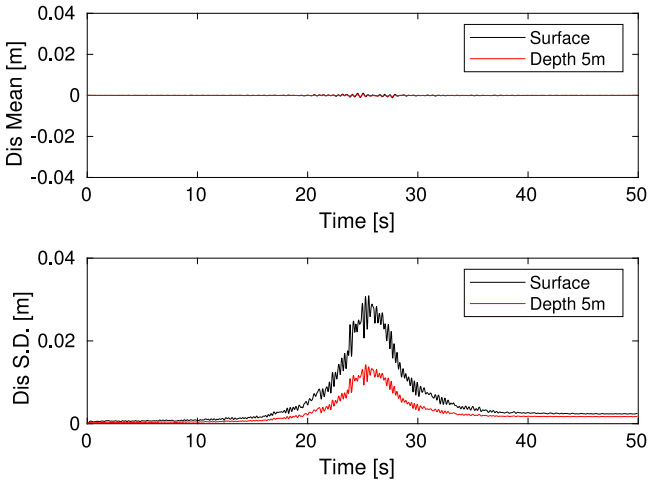


**Fig. 9.** Mean and standard deviation (S.D.) of the uncertain displacement at the ground surface and at the depth of 5 m.

The mean displacement and acceleration achieve significantly smaller values compared to the corresponding values of the standard deviation, both, at the ground surface and at the depth of 5 m. The response at the ground surface, in terms of the displacement and acceleration, is described by larger standard deviations than in the case of the response at the depth of 5 m. Apart from that, there is some uncertain permanent displacement, that is, a non-zero standard deviation of ground displacement at the end of the seismic loading. This is due to the material plastification.

With the results of the probabilistic site response represented by the Hermite PC expansion, any ground motion intensity measure commonly used in the probabilistic seismic hazard analysis (PSHA) can be obtained. For example, PDFs of the PGA and of the spectral acceleration, $Sa(T = 1.0\text{ s})$, at the ground surface and at the depth of 5 m are plotted in Fig. 11. PDF of the PGA from Fig. 11 shows the so-called fat-tailed characteristic, similarly as the one from Fig. 3 does. The PGA and the spectral acceleration, $Sa(T = 1.0\text{ s})$, at the ground surface have larger median values and more variability than those at the depth of 5 m.

The results from the MCS with 10,000 runs are also given in Figs. 10 and 11. In Fig. 10, it can be seen that both, the mean and the standard deviation, of the acceleration obtained from the SEPFE calculation are close to those obtained using the MCS. The SEPFE calculation results in a slightly larger variability, in terms of the standard deviation, than the MCS. Some discrepancies between the PDFs obtained from the SEPFE calculation and from the MCS can be seen in Fig. 11. For the mean response of surface PGA, there is 9% difference between SEPFEM and MCS. The mean response of surface acceleration $Sa(T = 1.0\text{ s})$ from SEPFEM is 8.3% higher than that from MCS. The differences can result from the error in the probabilistic discretization of PC-KL expansion as shown in Table 1, Figs. 6 and 8. The limited number of samples in MCS might have also contributed to the discrepancies between the results for SEPFEM and MCS.

Site-specific effects should be taken into account in the seismic ground motion modeling. Some empirical models have been proposed in the literature in order to account for the site amplification and non-linear effects in the case of a few intensity measures, like the PGA or the spectral acceleration, $Sa$, [54]. A site response analysis allows to investigate the site-specific effects in a more general and accurate way. Most of the current site response analyses are deterministic, however. Here, a framework for the elasto-plastic seismic site response analyses is used. It allows to account for the uncertainty in material properties and input motions. This framework can be successfully used in the site-specific PSHA. From the simulated site behavior, not only the PDF of any intensity measure but also the correlation between different intensity measures can be obtained. In Fig. 12, the joint PDF of the PGA and $Sa(T = 1.0\text{ s})$ for the probabilistic site response at the ground surface is plotted. The PGA and spectral acceleration $Sa(T = 1.0\text{ s})$ are positively correlated. The joint PDF and the correlation of intensity measures enable the vector-valued PSHA.

### 6.4. Sobol' sensitivity of the surface PGA

As per Section 5, Sobol' indices of surface PGA probabilistic response are calculated using the following input uncertainties, see Sections 6.1 and 6.2.

- Uncertain Soil Properties
  The initial shear stiffness of the soil is modeled as log-normally distributed random field with the marginal mean of 10 MPa and CV = 25%. The correlation structure is modeled using the exponential function with the correlation length of 15 m. The uncertain soil parameter, $H_a$, is represented using PC basis $\{\xi_1, \xi_2, \xi_3, \xi_4\}$ of dimension 4, order 2.
- Uncertain Input Seismic Motions
  Time-domain uncertain motions are simulated for a given earthquake scenario with $M = 8$, $R_{jb} = 12$ km and bedrock site condition $V_{s30} = 620$ m/s. The simulated uncertain motions are modeled as non-stationary, Gaussian random process with standard deviation $\sigma = 0.6$ for $\ln(\text{PGA})$ and represented with PC basis $\{\xi_5, \xi_6, \ldots, \xi_{104}\}$ of dimension 100, order 1.

From the computed Sobol' indices, the relative contributions of different input uncertainties to the variability of the output PGA at ground surface can be obtained.

- Contribution from Uncertain Soil Properties
  The total Sobol' index describing the contribution from the uncertain soil properties is $S^{PC,\text{total}}_{1,2,3,4} = 11.6\%$. The contribution to the total variance of the PGA from the uncertain soil properties only, i.e., excluding their interactions with the uncertain input motions, is 1.2%. The contribution from the interaction of the uncertainty

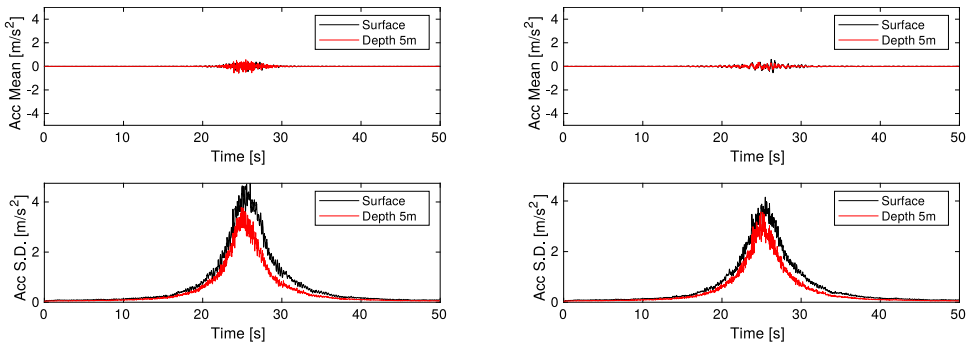


**(a)** SEPFE calculation **(b)** MCS

**Fig. 10.** Mean and standard deviation (S.D.) of the uncertain acceleration at the ground surface and at the depth of 5 m obtained from: (a) SEPFE calculation (b) MCS.

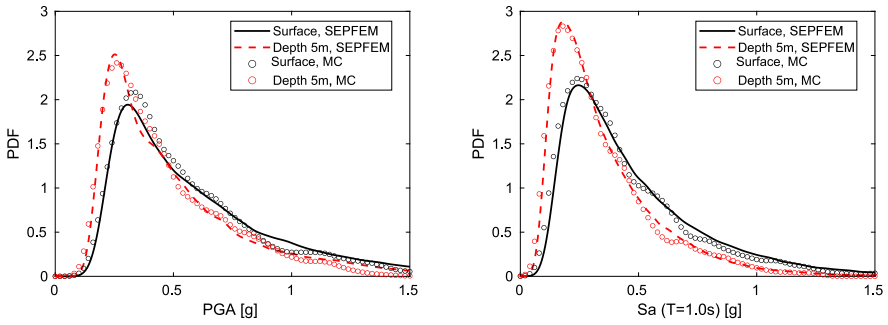


**(a)** PDF of PGA **(b)** PDF of $Sa(T = 1.0\ \mathrm{s})$

**Fig. 11.** PDFs of the PGA and of the spectral acceleration, $Sa(T = 1.0\ \mathrm{s})$, at the ground surface and at the depth of 5 m.

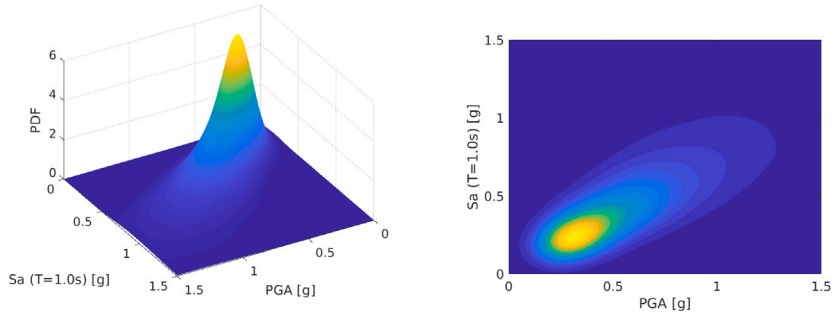


**(a)** Joint PDF of the PGA and $Sa(T = 1.0\ s)$ **(b)** Contour plot of the joint PDF

**Fig. 12.** Joint PDF of the PGA and the spectral acceleration, $Sa(T = 1.0\ s)$, for ground surface motions.

in the material parameters and in the input motions, i.e., contribution from the interacting PC components from both, $\{\xi_1, \xi_2, \xi_3, \xi_4\}$ and $\{\xi_5, \xi_6, \ldots, \xi_{104}\}$, is 10.4%. Sensitivity of the probabilistic system response to both, the individual uncertain material properties and input motions, as well as their combinations, should all be analyzed.

The Sobol' indices describing the contributions from the uncertain soil properties to the overall uncertainty in the PGA at the ground surface are given in Table 2.

- Contribution from Uncertain Input Motions

The total Sobol' index describing the contribution from the uncertain input motions is $S^{PC,\mathrm{total}}_{5,6,\ldots,104} = 98.8\%$. It is much larger than the contribution from the uncertain soil properties, i.e., 11.6%. The contribution to the total variance of the PGA from the uncertain input motions only, that is, excluding their interactions with the material parameters, is 88.4%. The contribution from these interactions is 10.4%.

The Sobol' indices describing the contributions from uncertain input motions to the uncertainty in the PGA at the ground surface are given in Table 3.

The total variability of the PGA is controlled mainly by the uncertain input motions. Such knowledge can be used in the engineering practice for the purpose of a better management of funds and time dedicated for the characterization of uncertain seismic input motions and uncertain soil properties. In this case, more resources should be prescribed to investigation of the uncertain input motions because they contribute to the overall variance of the PGA at the ground surface much more than the uncertain soil parameters do.

## 7. Conclusions

The Sobol' sensitivity analysis of a stochastic elasto-plastic seismic wave propagation was conducted using a novel numerical framework. The uncertain input bedrock motions and the uncertain elasto-plastic

**Table 2**
10 largest Sobol' indices describing the contributions of the uncertain soil properties to the uncertainty in the PGA at the ground surface.

| Sobol' index | Value |
|---|---|
| $S^{PC}_{1,8}$ | 0.034 |
| $S^{PC}_{1,6}$ | 0.013 |
| $S^{PC}_{1,10}$ | 0.011 |
| $S^{PC}_{1}$ | 0.009 |
| $S^{PC}_{1,14}$ | 0.009 |
| $S^{PC}_{1,17}$ | 0.007 |
| $S^{PC}_{1,13}$ | 0.007 |
| $S^{PC}_{1,15}$ | 0.006 |
| $S^{PC}_{1,12}$ | 0.005 |
| $S^{PC}_{1,5}$ | 0.003 |
| ... | ... |

**Table 3**
10 largest Sobol' indices describing the contributions of the uncertain input motions to the uncertainty in the PGA at the ground surface.

| Sobol' index | Value |
|---|---|
| $S^{PC}_{26}$ | 0.142 |
| $S^{PC}_{29}$ | 0.084 |
| $S^{PC}_{35}$ | 0.076 |
| $S^{PC}_{9}$ | 0.047 |
| $S^{PC}_{27}$ | 0.043 |
| $S^{PC}_{53}$ | 0.041 |
| $S^{PC}_{5}$ | 0.038 |
| $S^{PC}_{8}$ | 0.037 |
| $S^{PC}_{34}$ | 0.036 |
| $S^{PC}_{1,8}$ | 0.034 |
| ... | ... |

soil properties were modeled as a non-stationary random process and heterogeneous random fields, respectively. 1D probabilistic dynamic response of the soil was obtained using the SEPFEM. Through the probabilistic discretization of the uncertainties using the Hermite PC expansion, the probabilistic system response was obtained efficiently. The Sobol' indices were computed to evaluate the sensitivity of the system response to different uncertain inputs and their groups.

In this particular case, the uncertainty in the stochastic site response is mainly related to the uncertainty in the input motions. The combined uncertainty, in soil properties and motions, also significantly contributed to the overall uncertainty in the system response. The proposed calculation of the sensitivity of the system response to the individual uncertain inputs is very useful when making decisions about the distribution of funds in order to reduce the overall uncertainty in the predicted system response. Such influence should be analyzed for each case individually. The presented framework has been implemented into Real-ESSI Simulator [36] and it is available under http://real-essi.us/. In the future, the presented framework will be extended into a general 3D case, i.e., considering realistic, uncertain 3D heterogeneous site/geological conditions and 3D inclined, uncertain input motions.

## CRediT authorship contribution statement

**Hexiang Wang:** Writing – original draft, Validation, Software, Methodology, Investigation. **Fangbo Wang:** Writing – review & editing, Software, Methodology. **Han Yang:** Writing – review & editing, Software, Methodology. **Katarzyna Staszewska:** Writing – review & editing, Validation, Software, Methodology. **Boris Jeremić:** Writing – review & editing, Writing – original draft, Validation, Supervision, Software, Resources, Project administration, Methodology, Investigation, Funding acquisition, Conceptualization.

## Declaration of competing interest

The authors declare the following financial interests/personal relationships which may be considered as potential competing interests: Boris Jeremic reports financial support was provided by US Department of Energy. Boris Jeremic reports a relationship with US Department of Energy that includes: funding grants. If there are other authors, they declare that they have no known competing financial interests or personal relationships that could have appeared to influence the work reported in this paper.

## Acknowledgments

Financial support for presented work was provided by the USA Department of Energy (DE-AC02-05CH11231), University of California, Gdańsk University of Technology (DEC-014/2022/IDUB/II.1/AMERICIUM) and by personal funds from the senior Author.

## Data availability

Data will be made available on request.

## References

[1] Kramer SL. Geotechnical earthquake engineering. Upper Saddle River, New Jersey: Prentice Hall, Inc; 1996.
[2] Phoon K-K, Kulhawy FH. Characterization of geotechnical variability. Can Geotech J 1999;36:612–24.
[3] Phoon K-K, Kulhawy FH. Evaluation of geotechnical property variability. Can Geotech J 1999;36:625–39.
[4] Johari A, Amjadi A, Heidari A. Stochastic nonlinear ground response analysis: A case study site in Shiraz, Iran. Sci Iran 2021;28(4):2070–86. http://dx.doi.org/10.24200/sci.2021.55997.4507, arXiv:https://scientiairanica.sharif.edu/article_22130_77198ba46377a18c9b124af6b01ac475.pdf URL https://scientiairanica.sharif.edu/article_22130.html.
[5] Atik LA, Abrahamson N, Bommer JJ, Scherbaum F, Cotton F, Kuehn N. The variability of ground-motion prediction models and its components. Seismol Res Lett 2010;81(5):794–801.
[6] Amjadi AH, Johari A. Stochastic nonlinear ground response analysis considering existing boreholes locations by the geostatistical method. Bull Earthq Eng 2022;20(5):2285–327. http://dx.doi.org/10.1007/s10518-022-01322-1.
[7] Johari A, Vali B, Golkarfard H. System reliability analysis of ground response based on peak ground acceleration considering soil layers cross-correlation. Soil Dyn Earthq Eng 2021;141:106475. http://dx.doi.org/10.1016/j.soildyn.2020.106475, URL https://www.sciencedirect.com/science/article/pii/S0267726120311015.
[8] Kottke AR, Rathje EM. Technical manual for strata. Tech. rep., Berkeley, California: Pacific Earthquake Engineering Research Center; 2009.
[9] Sun Q, Guo X, Dias D. Evaluation of the seismic site response in randomized velocity profiles using a statistical model with monte carlo simulations. Comput Geotech 2020;120:103442. http://dx.doi.org/10.1016/j.compgeo.2020.103442, URL https://www.sciencedirect.com/science/article/pii/S0266352X20300057.
[10] Wang F, Sett K. Time-domain stochastic finite element simulation of uncertain seismic wave propagation through uncertain heterogeneous solids. Soil Dyn Earthq Eng 2016;88:369–85. http://dx.doi.org/10.1016/j.soildyn.2016.07.011, URL http://www.sciencedirect.com/science/article/pii/S0267726116300896.
[11] Wang H, Wang F, Yang H, Feng Y, Bayless J, Abrahamson NA, Jeremić B. Time domain seismic risk analysis framework for nuclear installations. In: Proceedings of the 25th international conference on structural mechanics in reactor technology. sMiRT 25, Charlotte, NC, USA; 2019, p. 8.
[12] Wang H, Wang F, Yang H, Feng Y, Bayless J, Abrahamson NA, Jeremić B. Time domain intrusive probabilistic seismic risk analysis of nonlinear shear frame structure. Soil Dyn Earthq Eng 2020;136:106201. http://dx.doi.org/10.1016/j.soildyn.2020.106201, URL http://www.sciencedirect.com/science/article/pii/S0267726119313016.
[13] Johari A, Momeni M. Stochastic analysis of ground response using non-recursive algorithm. Soil Dyn Earthq Eng 2015;69:57–82. http://dx.doi.org/10.1016/j.soildyn.2014.10.025, URL https://www.sciencedirect.com/science/article/pii/S0267726114002279.

[14] McKay MD. Evaluating prediction uncertainty. Tech. rep., Nuclear Regulatory Commission; 1995.
[15] Saltelli A, Tarantola S, Chan K-S. A quantitative model-independent method for global sensitivity analysis of model output. Technometrics 1999;41(1):39–56.
[16] Sobol I. Global sensitivity indices for nonlinear mathematical models and their Monte Carlo estimates. Math Comput Simulation 2001;55(1):271–80. http://dx.doi.org/10.1016/S0378-4754(00)00270-6, the Second IMACS Seminar on Monte Carlo Methods. URL http://www.sciencedirect.com/science/article/pii/S0378475400002706.
[17] Abbiati G, Marelli S, Tsokanas N, Sudret B, Stojadinović B. A global sensitivity analysis framework for hybrid simulation. Mech Syst Signal Process 2021;146:106997. http://dx.doi.org/10.1016/j.ymssp.2020.106997, URL https://www.sciencedirect.com/science/article/pii/S0888327020303836.
[18] Zeighami F, Sandoval L, Guadagnini A, Di Federico V. Uncertainty quantification and global sensitivity analysis of seismic metabarriers. Eng Struct 2023;277:115415. http://dx.doi.org/10.1016/j.engstruct.2022.115415, URL https://www.sciencedirect.com/science/article/pii/S0141029622014912.
[19] Bhattacharjee G, Baker JW. Using global variance-based sensitivity analysis to prioritise bridge retrofits in a regional road network subject to seismic hazard. Struct Infrastruct Eng 2023;19(2):164–77. http://dx.doi.org/10.1080/15732479.2021.1931892, arXiv:https://doi.org/10.1080/15732479.2021.1931892.
[20] Ghanem RG, Spanos PD. Stochastic finite elements, a spectral approach, revised edition edition. Dover Publications Inc.; 1991.
[21] Sakamoto S, Ghanem R. Polynomial chaos decomposition for the simulation of non-gaussian nonstationary stochastic processes. J Eng Mech 2002;128(2):190–201.
[22] Xiu D, Karniadakis GE. The Wiener–Askey polynomial chaos for stochastic differential equations. SIAM J Sci Comput 2002;24(2):619–44. http://dx.doi.org/10.1137/S1064827501387826.
[23] Xiu D, Karniadakis GE. Modeling uncertainty in flow simulations via generalized polynomial chaos. J Comput Phys 2003;187(1):137–67.
[24] Oladyshkin S, Nowak W. Data-driven uncertainty quantification using the arbitrary polynomial chaos expansion. Reliab Eng Syst Saf 2012;106:179–90. http://dx.doi.org/10.1016/j.ress.2012.05.002, URL http://www.sciencedirect.com/science/article/pii/S0951832012000853.
[25] Jakeman JD, Franzelin F, Narayan A, Eldred M, Plfüger D. Polynomial chaos expansions for dependent random variables. Comput Methods Appl Mech Engrg 2019;351:643–66. http://dx.doi.org/10.1016/j.cma.2019.03.049, URL http://www.sciencedirect.com/science/article/pii/S0045782519301884.
[26] Ghanem R, Kruger RM. Numerical solution of spectral stochastic finite element systems. Comput Methods Appl Mech Engrg 1996;129(3):289–303. http://dx.doi.org/10.1016/0045-7825(95)00909-4.
[27] Ghanem R. Ingredients for a general purpose stochastic finite elements implementation. Comput Methods Appl Mech Engrg 1999;168(1–4):19–34.
[28] Matthies HG, Brenner CE, Bucher CG, Soares CG. Uncertainties in probabilistic numerical analysis of structures and solids – stochastic finite elements. Struct Saf 2004;19(3):283–336.
[29] Matthies HG, Keese A. Galerkin methods for linear and nonlinear elliptic stochastic partial differential equations. Comput Methods Appl Mech Engrg 2005;194(1):1295–331.
[30] Sett K, Jeremić B, Kavvas ML. Stochastic elastic–plastic finite elements. Comput Methods Appl Mech Engrg 2011;200(9–12):997–1007. http://dx.doi.org/10.1016/j.cma.2010.11.021.
[31] Karapiperis K, Sett K, Kavvas ML, Jeremić B. Fokker-planck linearization for non-gaussian stochastic elastoplastic finite elements.. Comput Methods Appl Mech Engrg 2016;307:451–69.
[32] Wang F, Sett K. Time domain stochastic finite element simulation towards probabilistic seismic soil–structure interaction analysis. Soil Dyn Earthq Eng 2019;116:460–75. http://dx.doi.org/10.1016/j.soildyn.2018.10.021, URL http://www.sciencedirect.com/science/article/pii/S0267726118306365.
[33] Sudret B. Global sensitivity analysis using polynomial chaos expansions. Reliab Eng Syst Saf 2008;93(7):964–79.
[34] Bora SS, Scherbaum F, Kuehn N, Stafford P, Edwards B. Development of a response spectral ground-motion prediction equation (GMPE) for seismic-hazard analysis from empirical fourier spectral and duration models. Bull Seismol Soc Am 2015;105(4):2192–218.
[35] Stafford PJ. Interfrequency correlations among fourier spectral ordinates and implications for stochastic ground-motion simulationinterfrequency correlations among fourier spectral ordinates and implications. Bull Seismol Soc Am 2017;107(6):2774–91.
[36] Jeremić B, Jie G, Cheng Z, Tafazzoli N, Tasiopoulou P, Pisanò F, Abell JA, Watanabe K, Feng Y, Sinha SK, Behbehani F, Yang H, Wang H, Staszewska KD. The real-ESSI simulator system. Davis: University of California; 1988-2024, http://real-essi.us/.
[37] Gregor N, Abrahamson NA, Atkinson GM, Boore DM, Bozorgnia Y, Campbell KW, Chiou BS-J, Idriss I, Kamai R, Seyhan E, et al. Comparison of NGA-West2 GMPEs. Earthq Spectra 2014;30(3):1179–97.
[38] Boore DM. Simulation of ground motion using the stochastic method. Pure Appl Geophys 2003;160:635–76.
[39] Bora SS, Cotton F, Scherbaum F. NGA-West2 empirical fourier and duration models to generate adjustable response spectra. Earthq Spectra 2018;2.
[40] Bayless J, Abrahamson NA. Summary of the ba18 ground-motion model for fourier amplitude spectra for crustal earthquakes in california. Bull Seismol Soc Am 2019;109(5):2088–105.
[41] Bayless J, Abrahamson NA. Evaluation of the interperiod correlation of ground-motion simulations. Bull Seismol Soc Am 2018;108(6):3413–30.
[42] Bayless J, Abrahamson NA. An empirical model for the interfrequency correlation of epsilon for fourier amplitude spectra. Bull Seismol Soc Am 2019;109(3):1058–70.
[43] Boore DM. Phase derivatives and simulation of strong ground motions. Bull Seismol Soc Am 2003;93(3):1132–43.
[44] Baglio MG. Stochastic ground motion method combining a Fourier amplitude spectrum model from a response spectrum with application of phase derivatives distribution prediction. (Ph.D. thesis), Politecnico di Torino; 2017.
[45] Rezaeian S, Petersen MD, Moschetti MP, Powers P, Harmsen SC, Frankel AD. Implementation of NGA-West2 ground motion models in the 2014 US national seismic hazard maps. Earthq Spectra 2014;30(3):1319–33.
[46] Jeremić B, Yang Z, Cheng Z, Jie G, Tafazzoli N, Preisig M, Tasiopoulou P, Pisanò F, Abell J, Watanabe K, Feng Y, Sinha SK, Behbehani F, Yang H, Wang H, Staszewska KD. Nonlinear finite elements: modeling and simulation of earthquakes, soils, structures and their interaction, self-published-online. University of California, Davis, CA, USA; 1989–2024, uRL: http://sokocalo.engr.ucdavis.edu/jeremic/LectureNotes/.
[47] Chopra AK. Dynamics of structures, theory and application to earthquake engineering. second ed.. Prentice Hall; 2000.
[48] Newmark NM. A method of computation for structural dynamics. ASCE J Eng Mech Div 1959;85:67–94.
[49] Armstrong P, Frederick C. A mathematical representation of the multiaxial bauschinger effect.. Technical Report RD/B/N/ 731, C.E.G.B., 1966.
[50] Pisanò F, Jeremić B. Simulating stiffness degradation and damping in soils via a simple visco-elastic–plastic model. Soil Dyn Geotech Earthq Eng 2014;63:98–109.
[51] Lebrun R, Dutfoy A. An innovating analysis of the nataf transformation from the copula viewpoint. Probab Eng Mech 2009;24(3):312–20.
[52] Jiang SH, Huang J, Huang F, Yang J, Yao C, Zhou CB. Modelling of spatial variability of soil undrained shear strength by conditional random fields for slope reliability analysis. Appl Math Model 2018;63:374–89.
[53] Argyris J, Mlejnek H-P. Dynamics of structures. North Holland in USA Elsevier; 1991.
[54] Kamai R, Abrahamson NA, Silva WJ. Nonlinear horizontal site amplification for constraining the NGA-West2 GMPEs. Earthq Spectra 2014;30(3):1223–40.